Available online at www.sciencedirect.com
SCIENCE DIRECT®
Thermochimica Acta 433 (2005) 187–195
thermochimica acta
www.elsevier.com/locate/tca

Clay intercalation and influence on crystallinity of EVA-based clay nanocomposites

D.S. Chaudhary, R. Prasad, R.K. Gupta, S.N. Bhattacharya *

Rheology and Materials Processing Centre, School of Civil and Chemical Engineering, RMIT University, 124 La Trobe St., Melbourne 3000, Australia

Received 7 December 2004; received in revised form 4 February 2005; accepted 14 February 2005
Available online 26 April 2005

Abstract

Various polymer clay nanocomposites (PCNs) were prepared from ethylene vinyl acetate copolymer (EVA) with 9, 18 and 28% vinyl acetate (VA) content filled with different wt.% (2.5, 5 and 7.5) of a Montmorillonite-based organo-modified clay (Cloisite® C15A and C30B). The PCNs were prepared using melt blending techniques. Morphological information regarding intercalation and exfoliation were determined by using wide-angle X-ray scattering (WAXS) and transmission electron microscopy (TEM). WAXS and TEM confirmed that increasing the VA content was necessary to achieve greater clay–polymer interaction as seen from the comparatively higher intercalation of clay platelets with 28% VA. The effect of addition of clay on the development and the modification of crystalline morphology in EVA matrix was also studied using WAXS and temperature-modulated differential scanning calorimetry (MDSC). Results are presented showing that the addition of clay platelets does not increase the matrix crystallinity but the morphology was significantly modified such that there was an increase in the 'rigid' amorphous phase. Mechanical properties were also evaluated against the respective morphological information for each specimen and there are indications that the level of clay–polymer interaction plays a significant role in such morphological modification, and in such a way that affects the final PCN mechanical properties which has wide and significant applications in the packaging industries.

Keywords: EVA; Nanocomposites; Mechanical; Morphology; MDSC

1. Introduction

The combination of ethylene vinyl acetate (EVA) with nanoclay has wide commercial applications (such as packaging films, cables and adhesives), and these applications depend on the vinyl acetate (VA) contained in the main chain. As the VA content increases, the copolymer presents increasing polarity but lower crystallinity, and therefore different mechanical behavior [1]. The increasing polarity with increasing VA content is apparently useful in imparting a high degree of polymer–clay surface interaction, and it has been reported that there is a significant rise in the Young's modulus and the yield strength of the EVA PCNs [2], in tune with the behavior of other polymeric nanocomposites [3].

This study is aimed at producing EVA nanocomposites using matrices with various VA content and clay concentrations, and analyzing them for their respective clay–polymer interaction and their influence on the phase modification (matrix crystallinity) and mechanical properties. Since the VA content dictates the polarity of the matrix – thus dictating the level of organoclay–polymer interaction – morphologies of EVA nanocomposites would differ based on VA content and their interaction with its nanoclay content. For example, some authors have reported how the structure–mobility properties of EVA polymer are influenced by the VA content [4] and this chain mobility in and around clay galleries could significantly modify the level of interaction in clay nanocomposites. Also, it is well known that inclusion of filler provides a suitable pathway for increased crystallinity and consequently higher crystallization temperatures in polymeric samples because of the nucleation effects of the fillers (by providing active surface structures) [5]. However, presence of small quan-

* Corresponding author. Tel.: +61 3 992552086; fax: +61 3 99252268.
E-mail addresses: deeptangshu@hotmail.com (D.S. Chaudhary), sati.bhattacharya@rmit.edu.au (S.N. Bhattacharya).

0040-6031/$ – see front matter © 2005 Elsevier B.V. All rights reserved.
doi:10.1016/j.tca.2005.02.031

tity of nanoclay may not increase the matrix crystallinity as it might be 'rejected' during crystallization as impurity and may result in a significant increase in the amorphous 'bulk'. Such changes in polymer clay nanocomposite (PCN) morphology would bring about a change in their mechanical properties, for example, presence of a well-dispersed clay platelet network in the amorphous bulk could increase the elastic response by providing a 'solid network'. With EVA, it is interesting to investigate the dominance of its polarity and clay interaction and the changes in the crystallinity of EVA nanocomposites.

2. Experimental

2.1. Nanocomposite preparation

EVA copolymer with 9, 18 and 28% VA was supplied by Dupont, Australia. The molecular weights are 67320, 72600 and 58300, respectively, with polydispersity of 4.6, 8.7 and 6.2, respectively. Two organo-modified MMT clay were used as received; Cloisite® 15A (C15A) and Cloisite® 30B (C30B) by Southern Clay Products (Gonzales, USA). C15A was produced by modifying hydrophilic Na^+-MMT by using the dimethyl dihydrogenated, tallow quaternary ammonium chloride and is more suitable for less polar EVA9 due to long aliphatic chains in C15A. C30B was produced by modifying hydrophilic Na^+-MMT with methyl, tallow and bis-2-hydroxyethyl quaternary ammonium. This group of modified clays is suitable for the more polar polymers like EVA18 and EVA28. Composites with varying filler level (2.5, 5 and 7.5%, w/w) were prepared using the melt blending technique using an intermeshing counter-rotating twin-screw extruder (Brabender, Duisburg, Germany).

2.2. Mechanical characterization

Test specimens conforming to ASTM 638M were cut from the plaques made by compression molding of the PCN samples at 120 °C and under 12 KN. The mixing and molding conditions were identical for all samples. At least six samples were subjected to tensile test on an Instron Universal Testing Machine (model: 4467, Instron Corporation, UK).

2.3. Morphological characterization

2.3.1. WAXS

Wide-angle X-ray scattering (WAXS) experiments on a 2-mm thick sample, placed in a rotating holder – to eliminate effects of structural orientation in the sample during a transmission test [6] – were conducted using a Philips X-ray generator with 30 kV accelerating voltage and 30 mA current (Philips PW 1130, Holland). Intensities from $2\theta = 1.2°$–$35°$ were recorded using Ni-filtered Cu Kα radiation ($\lambda = 0.154$ nm) and d_{001} spacing was found using Bragg's law ($\lambda = 2d_{001} \sin\theta$). Background radiation has been removed from the scattering curves to be able to show scattering intensities up to 2θ of about 1.3°.

2.3.2. TEM

Transmission electron microscopy (TEM) analysis was used to provide a 'visual' confirmation of the morphological information obtained on the platelet dispersion and distribution from the WAXS data as the latter lacks the ability to characterize the disordered-intercalated or the exfoliated structures due to the absence of scattered intensity peaks for those morphologies [7]. Ultra-thin sections measuring approximately 70 nm were ultra-microtomed by using a diamond knife at approximately (−)165 °C and samples were placed on copper grids to be viewed under a JEOL TEM equipment with an accelerating voltage of 100 kV and high vacuum (JEOL 1010, Japan).

2.3.3. MDSC

Samples for modulated differential scanning calorimetry (MDSC, DSC 2920 *modulated* DSC with Thermal Analyst 3100 software, TA Instruments, USA) were prepared from the specimen by compression molding into thin films (thickness < 1 mm) and the tests were conducted using helium as purge gas (30 ml/min flowrate) and nitrogen as environment gas (100 ml/min flowrate) with at least two specimens for each sample to ensure the repeatability. The heating and cooling rate were constant at 2 °C/min using 0.5 °C modulation amplitude and at a 40-s modulation period. The results were analysed from the second heating and cooling curves. The stability of any particular clay–polymer system was determined after comparing the crystallization enthalpy and the temperatures of the first and second cooling curves. Enthalpies of melting and crystallization, along with the respective temperatures, were obtained by using the peak integration method. The non-isothermal crystallization kinetics for various EVA PCNs were studied using modified Avrami equation.

3. Results and discussion

3.1. WAXS analysis

WAXS data shown in Fig. 1 have been discussed in detail previously [2]. Pristine C15A clay was found to have $d_{001} = 3.52$ nm as compared to the swelled EVA9 PCNs with 4.64 nm (2.5%), 4.41 nm (5%) and 3.92 nm (7.5%). The WAXS data show that the peak intensity of 2.5% C15A has been significantly reduced and shifted towards lower angles, but the peak is not as broad as with 5% or 7.5% indicating that in 2.5%, the tactoids separate into platelets with comparatively larger gallery space and maintain their ordered structure in the smaller scale. However, the second peak intensities in 2.5% is insignificant as compared to 5% or 7.5% indicating that in PCNs with the latter two concentrations, the comparatively higher concentration of clay could not be exfoliated but in general, small groups of layered silicates in a tactoid

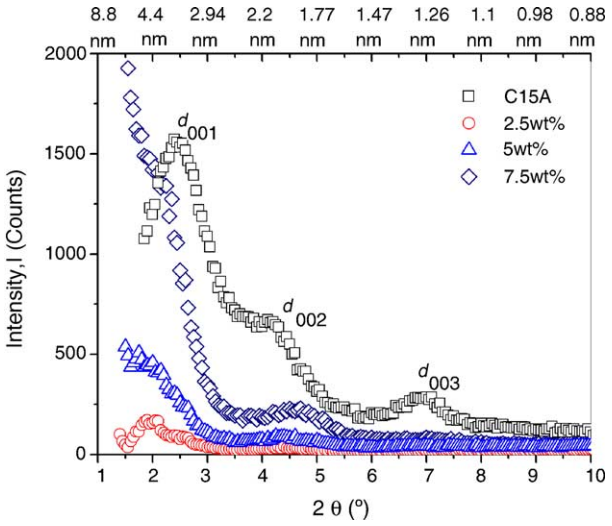

Fig. 1. WAXS patterns comparing the nature of intensity and *d*-spacing of C15A as well as EVA9-C15A nanocomposites at clay loading of 2.5, 5 and 7.5 wt.%.

would have become more disordered and randomly oriented, while maintaining a periodicity within the platelets giving a highly diffused band at higher angles. Such characteristics have been dealt similarly in other's interpretation [8].

The absence of any peak for all clay concentrations in Fig. 2 indicates that significant intercalation and/or exfoliation have been achieved for EVA18 PCNs. Apparently, an increase in the content of polar VA groups in EVA18 as compared to EVA9, which lowered the thermodynamic energy barrier for clay–polymer interaction, possibly allowed a relatively higher number of polymer chains to migrate and stabilize within the clay platelet galleries and form partially exfoliated [3] and/or disordered-intercalated states [9]. Further evidence towards the primary morphology can be gained from TEM analysis.

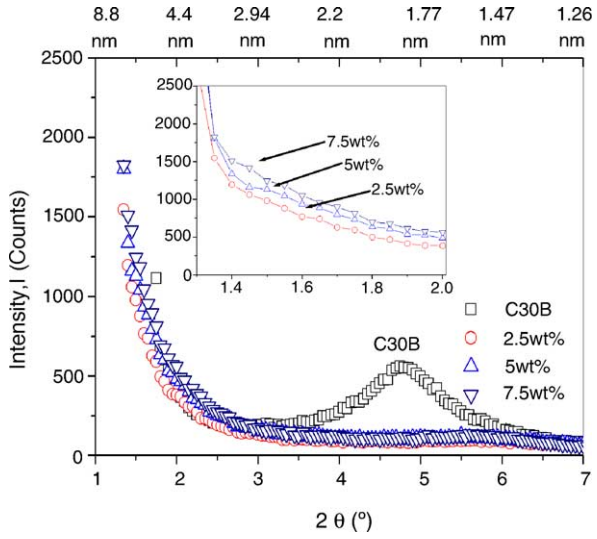

Fig. 2. WAXS patterns comparing the nature of intensity and *d*-spacing of C30B as well as EVA18-C30B nanocomposites at clay loading of 2.5, 5 and 7.5 wt.%.

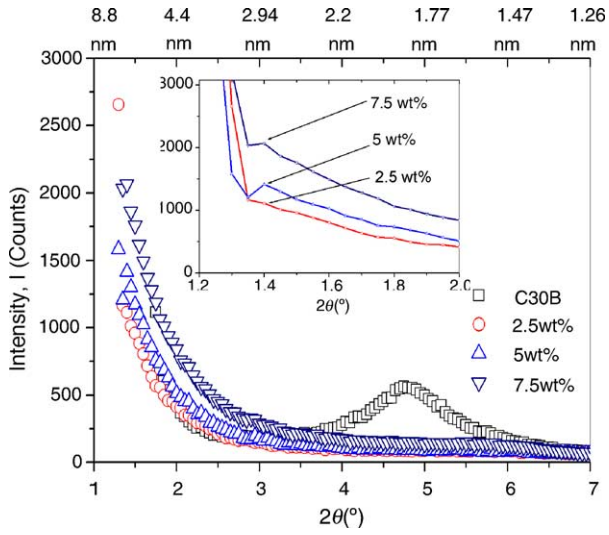

Fig. 3. WAXS patterns comparing the nature of intensity and *d*-spacing of C30B as well as EVA28-C30B nanocomposites at clay loading of 2.5, 5 and 7.5 wt.%.

Fig. 3 shows that all EVA28 PCNs have a low intensity shoulder at $2\theta = 1.4^\circ$ ($d_{001} = 6.3$ nm) indicating a high degree of platelet incoherence or a 'highly exfoliated system' [3] when compared to pristine clay ($d_{001} = 1.86$ nm). It is thought that the increased polarity of the polymer chains could have facilitated polymeric chain stabilization within the clay galleries. Similar effects are also seen for EVA18 PCNs, and the stabilization could be due to the higher amorphous content (due to the increased VA groups) that prevents it from re-crystallizing during annealing and allowed the polymeric chains to remain diffused within clay platelets. However, WAXS is not capable of confirming whether the platelet incoherence has resulted in a highly disordered-intercalated or exfoliated morphology.

Being low viscous EVA28, though gave a high basal spacing, probably has lower shear action, which could limit the degree of clay platelet 'randomization'. For lower clay concentration, this might not be of significant issue; however, at comparatively higher concentrations – and considering good platelet exfoliation – the EVA28 might not be effective in 'randomizing' platelets due to an apparent 'saturation effect', where the free spatial movement of individual clay platelet might be limited by an increased presence of highly interacting VA "pendants" tying up with individual platelets creating clay–polymeric chain domains. This probably causes a highly disordered-intercalated morphology and this can be seen for all clay concentrations as shown by the inset of Fig. 3. It is interesting that EVA18 PCNs, did exhibit similar behaviour at all the scattering angles because of the lower density of 'pendants' in EVA18 and its capability to accept the greater clay volume, which resulted in a high degree of platelet dispersion in the matrix. Detailed WAXS and TEM analyses on the intercalation and exfoliation of EVA-clay (Cloisite®) system have been dealt in another article [10].

3.2. TEM analysis

Figs. 4a–c, 5a–c and 6a–c illustrate the TEM micrographs for EVA9, EVA18 and EVA28 nanocomposites, respectively. The higher electron density of the silicates relative to the EVA matrix gives them a much darker appearance. TEM images for EVA9 nanocomposites show the presence of tactoids that are approximately 200 nm thick and this suggests that for EVA9-C15A system, the clay platelets are not dispersed fully, possibly due to the low matrix polarity. However, the tactoids themselves gain some degree of disorderness, which is strongly affected by the clay concentration. This agrees very well with WAXS data as shown in Fig. 1 that showed Bragg peaks and rules out exfoliation.

The absence of Bragg peaks in EVA18 nanocomposites WAXS (Fig. 2) suggested that it exhibits mixed exfoliated or disordered-intercalated morphologies. This is strongly supported by the TEM images shown in Fig. 5a–c. The presence of stacks of silicate layers at higher concentration shows the presence of intercalation, where few platelets are grouped together but possess random orientations, whereas at lower concentrations (2.5% and 5%), the clay platelets are scattered individually while some tactoid-structural orderness is preserved suggesting mixed exfoliation. Larger particles could also be observed and these may be the tactoids that have not been dispersed well enough. Similar morphologies for EVA18-based nanocomposites were reported by Gilman et al. [11] and it was shown earlier that these morphologies influence the melt behavior significantly [10].

Fig. 6a–c reveals that for EVA28 nanocomposites, exfoliated individual layers are interspersed with silicate stacks that are a few layers thick. The TEM images of EVA28 also show that increasing silicate loading from 2.5 to 7.5 wt.% does not affect the dispersion of platelets – the level of exfoliation remains high – indicating that with increased polarity of the matrix (28% VA), increased clay–polymer interaction takes place.

3.3. MDSC analysis

From Fig. 7, it can be seen that the melting endotherm is significantly affected by the VA content; the broad endotherm for EVA28 appears more like a 'bump' and is contrasting to the broad but defined endotherm of EVA9. Fig. 8 shows typical heat flow curve (second heating and cooling) for EVA28 PCNs and it can be seen from the cooling curve that the crystallization process for EVA28 is significantly affected by the presence of clays. As widely known, in polymer–clay systems, the clay platelets are in nano dimensions and the interactions are at molecular levels. Upon baseline calibration, the endotherm can suggest the information about the crystalline phase in the nanocomposites. For example, the clay is known to increase the crystallization rate and has a strong heterophase nucleation effect on Nylon 6 [12], where random orientation of clay platelets caused a high molecular interactions and resulted in formation of crystals with a size distribution depending upon the clay–polymer and polymer–polymer interaction. During heating, some of these thin crystals are partially melted and the progressive movement of the clays platelets gives them the sufficient entropy to coalesce (re-crystallize) and rearrange to form larger crystals that are eventually melted at slightly higher temperature. Also, since the growth of crystal structure is hindered but interestingly the total crystallinity is seldom affected [13], it is suggested that the apparent volume of the crystals is reduced in the matrix.

Non-isothermal crystallization kinetics were studied using the modified Avrami equation and assuming that the crystallization process is a combination of several infinitesimally small isothermal steps such that the development of relative crystallinity can be expressed as [14]

$$Xt = \int_{t_0}^{t} \frac{\mathrm{d}H_c}{\mathrm{d}t}\mathrm{d}t \Big/ \int_{t_0}^{t_\infty} \frac{\mathrm{d}H_c}{\mathrm{d}t}\mathrm{d}t$$

All the curves have a partial sigmoidal shape (not shown here) and the analysis of the development of relative crystallinity can be done using

$$Xt = 1 - \exp(-kt^n)$$

A plot of $\log[-\ln(1 - Xt)]$ versus $\log(t)$ can then provide n, the value depending upon the mechanics of nucleation and on the form of crystal growth; and k, a rate constant containing the nucleation and growth parameters. The Avrami plots for EVA9, 18 and 28 PCNs are shown in Figs. 9–11, respectively. It can be seen that except for EVA9 PCNs, the other plots are straight lines over a relatively wide crystalline range, with EVA28 PCNs showing the most linearity. The non-linearity of the plots could be attributed to the presence of secondary crystallization phenomenon as reported for other PCN systems [15]. This indicates that modified Avrami equation can describe the non-isothermal crystallization process of the EVA PCNs with relatively higher VA content (viz., 18% and 28%). The exponent n is tabulated in Table 1 for EVA9, 18 and 28 PCNs, respectively and the rate constant k is discussed later.

For EVA9, the plots in Fig. 9 have apparently two linear regions; the difference in the slope of the first and the second region indicates the onset of a typical heterogeneous nucleation with melting of recently formed smaller imperfect crystals. Progressive re-crystallization leads to slow one-dimensional growth as the fractional crystallinity increases in the sample. This may be due to the presence of smaller clay tactoids (seen in TEM) that can cause apparent rapid crystallization (by restricting the polymer motion), but further platelet movement would cause the chains to reorganize more uniformly and allow crystal growth. In other words, as heat is being extracted from the system, chains under the obstructive influence of clay platelets (spatial hindrances) imperfectly orient and assemble and creating a peudo-organisation (small crystalline regions); however, as the clay also moves and orients progressively in the bulk, some chains gain entropy and as further heat is extracted, these chains favorably orients towards the

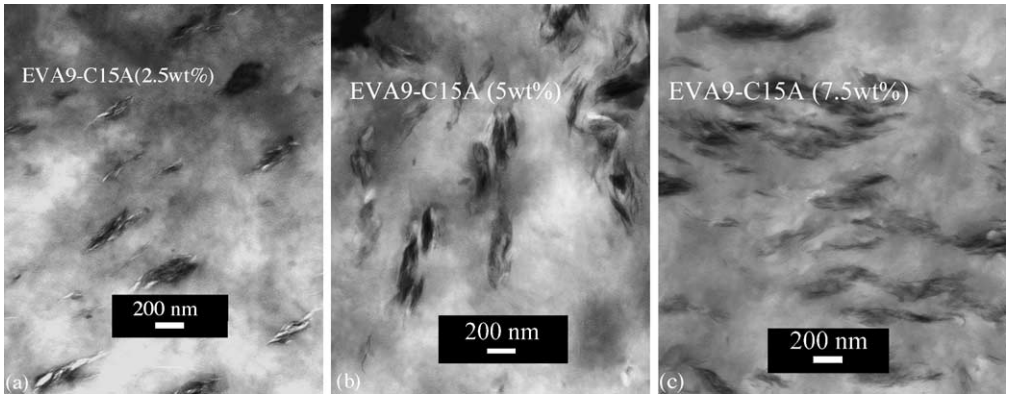

Fig. 4. TEM micrographs of (a) 2.5 wt.%; (b) 5 wt.% and (c) 7.5 wt.% EVA9-C15A nanocomposites.

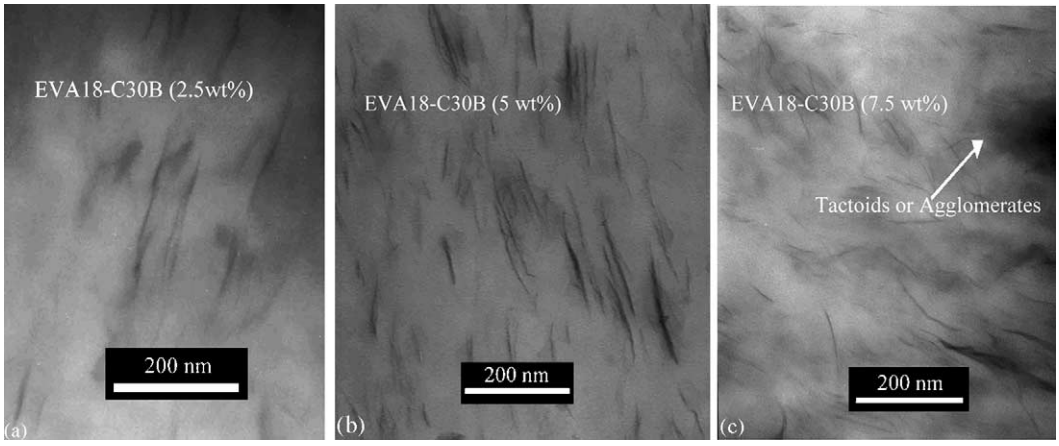

Fig. 5. TEM micrographs of (a) 2.5 wt.%; (b) 5 wt.% and (c) 7.5 wt.% EVA18-C30B nanocomposites.

bulk and assembles with greater organisation. As such, there is a complex growth mechanism, and therefore, EVA9 PCNs do not completely conform to Avrami equation.

For EVA18 and EVA28 PCNs, there exist similar secondary crystallization phenomenon (as seen in EVA9) but the Figs. 10 and 11 show that there is a relatively larger linear region and the value of n for all clay content range from 1.3 to 3.2 indicating the heterogeneous nucleation. However, the data in Table 1 show that the clay platelets may act as nucleating agents and not hinder the lamella growth but only for EVA9 PCNs with 5 and 7.5 wt.% clay (n values for PCNs are higher than for pure polymer) whereas for EVA18 or EVA28 PCNs, the exfoliated clay platelets simply reorganize to form a 'network' structure that suppresses the crystallinity.

The above argument was corroborated by measuring the sample crystallinity from the total enthalpy data for all EVA PCNs. As shown in Fig. 12, the fractional crystalline morphology does not change significantly for EVA9 PCNs – all samples ∼33% crystallinity – whereas, there is ∼40% reduction in total crystalline morphology for EVA28 PCNs and

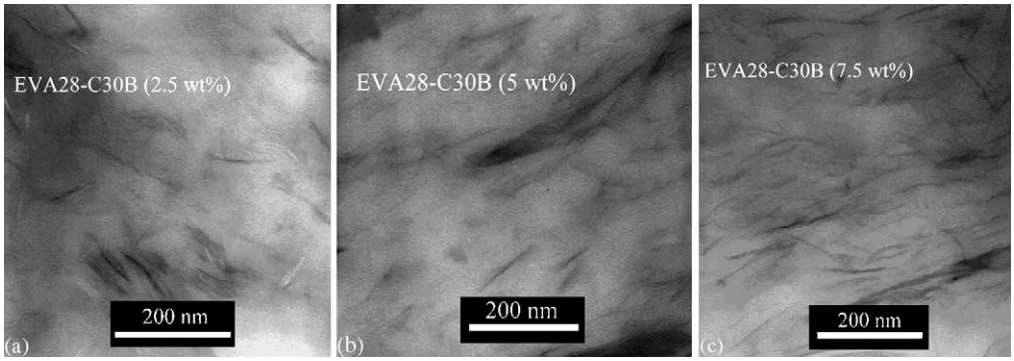

Fig. 6. TEM micrographs of (a) 2.5 wt.%; (b) 5 wt.% and (c) 7.5 wt.% EVA28-C30B nanocomposites.

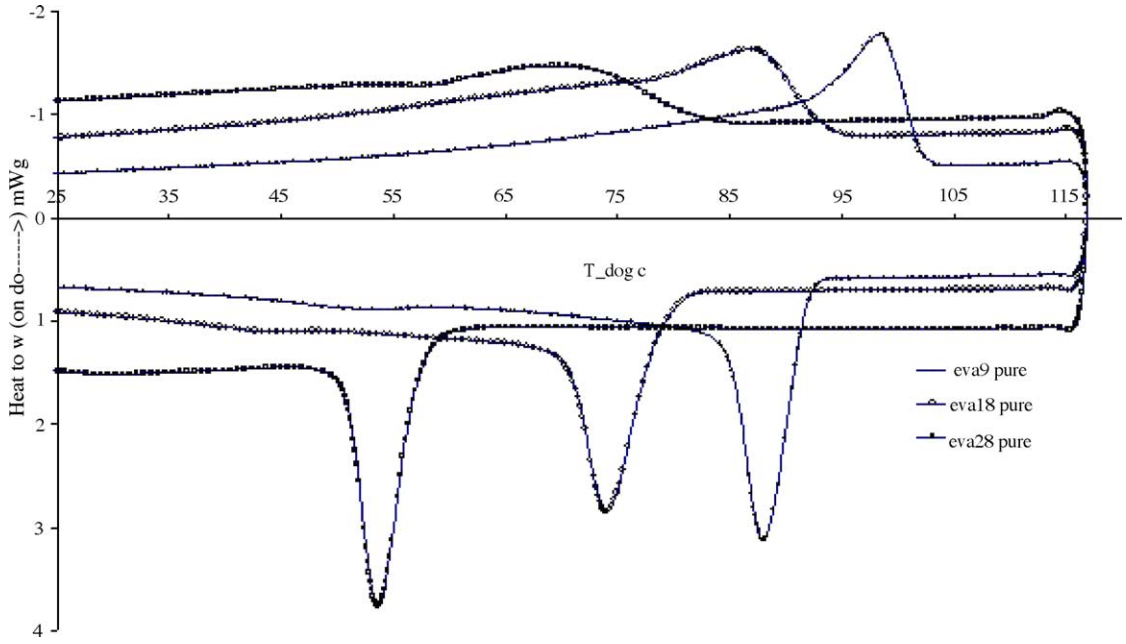

Fig. 7. Typical heat flow curve (second heating and cooling) for pure EVA polymers.

∼30% reduction in EVA18-2.5 and EVA18-5 with EVA18-7.5 showing the highest reduction at ∼60%. Such morphological change is expected to bring about a significant rise in the mechanical properties, especially the strength of the PCNs, since it is well known that the clay platelets can act as a reinforcing agent.

Moreover, since the rate constant *k* obtained from the intercept does not have the same physical meaning as in isothermal conditions (the temperature is continuously changing in non-isothermal conditions), we attempt to understand the rate kinetics by considering the exotherm slope of the various PCNs. From the 'slope' values in Fig. 13, it is seen that the addition of clays significantly reduce the growth rate for all EVA PCNs, possibly due to modification to the nucleation mechanism, and interestingly the effect is pronounced for EVA9 PCNs. It is very likely that there could be formation of a 'network' structure of platelets with increasing clay content – 'network' involves platelet–platelet interaction apart from the platelet–polymer interaction – and this intercalation increases the total entanglement volume. The onset of such structure

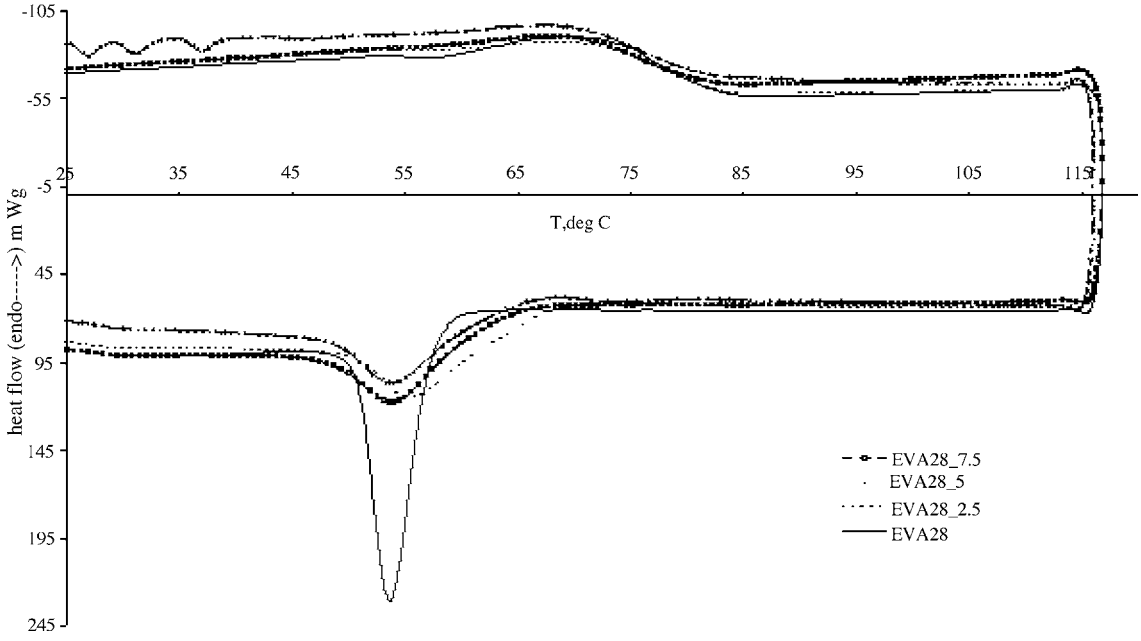

Fig. 8. Typical second heat flow curve for EVA28 PCNs along with the pure polymer.

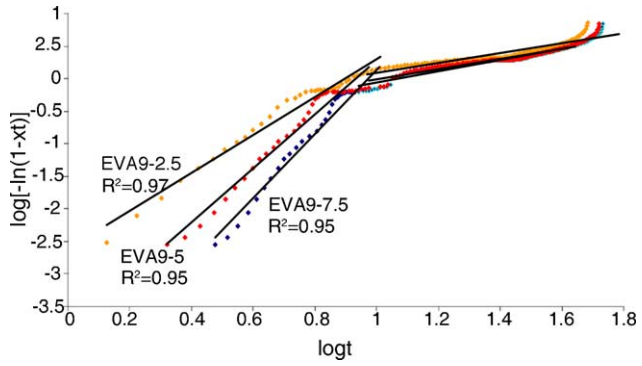

Fig. 9. Plot of log(t) vs. log log[$-\ln(1-Xt)$] for EVA9 PCNs for non-isothermal conditions.

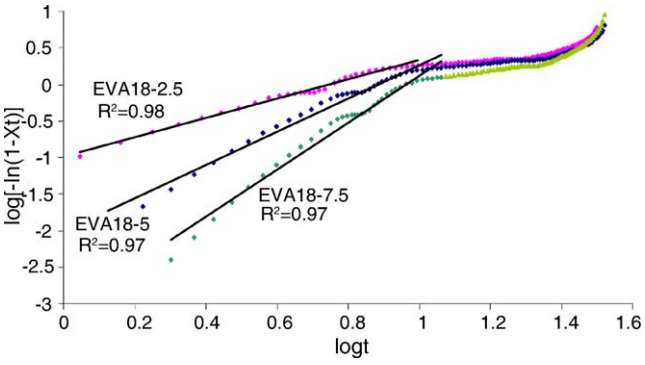

Fig. 10. Plot of log(t) vs. log log[$-\ln(1-Xt)$] for EVA18 PCNs for non-isothermal conditions.

could be seen in light of percolation threshold – thus polymer chains are entangled within platelet structures – forming a non-mobile amorphous phase, which reduces the fractional crystalline morphology. This is suggested for EVA18 and 28 (Fig. 12), but may not occur in EVA9, where matrix crystallization processes 'encompasses' clay tactoidal-structures. Further studies in melt state properties are required to gain understanding of such 'network' morphology, and are being carried out currently. An important aspect of these results is that it is not system-specific, and the analysis points out the significance of the level of clay–polymer interaction and matrix polarity in determining the final composite morphology, which is more suitable for stretch-film packaging.

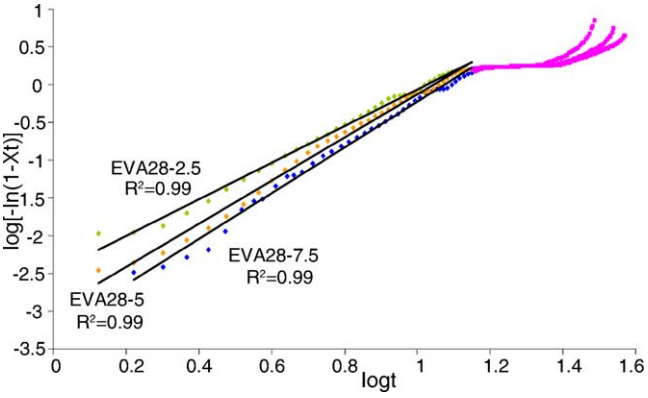

Fig. 11. Plot of log(t) vs. log[$-\ln(1-Xt)$] for EVA28 PCNs for non-isothermal conditions.

Table 1
Parameter n determined using the modified Avrami equation for all EVA PCNs

Sample name	Clay (wt.%)	n
EVA9-0	0	3.8
EVA9-2.5	2.5	2.9
EVA9-5	5	4.1
EVA9-7.5	7.5	4.8
EVA18-0	0	4.6
EVA18-2.5	2.5	1.3
EVA18-5	5	2.3
EVA18-7.5	7.5	3.2
EVA28-0	0	4.5
EVA28-2.5	2.5	2.4
EVA28-5	5	2.8
EVA28-7.5	7.5	3.0

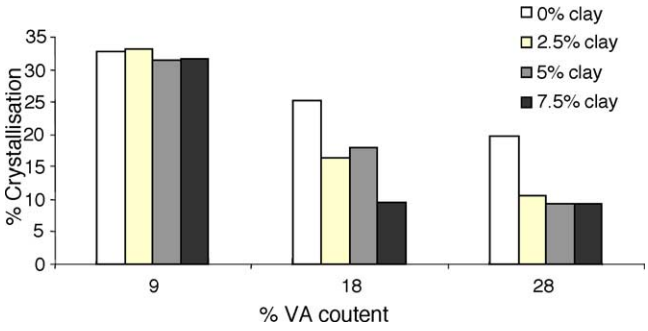

Fig. 12. The fractional crystalline morphologies of the pure polymer and the EVA PCNs.

3.4. Tensile analysis

In EVA with increasing VA content, the crystallinity of the polymer decreases (and will lower the stiffness), while the polarity increases (and will increase the intercalation). Therefore, in the present system, the stiffness and toughness response would be an interplay of two factors: (a) an increase in the 'rigid' amorphous phase due to polymer–clay interca-

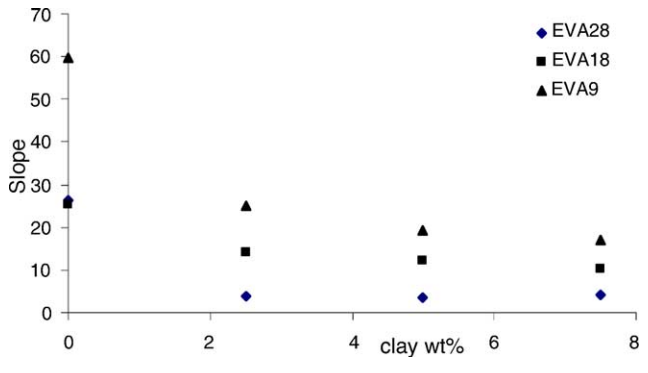

Fig. 13. 'Slope' derived from the exotherm curve of the second cooling cycle for all EVA PCNs. Here the physical meaning of slope has been interpreted in terms of having the nucleation and growth parameters.

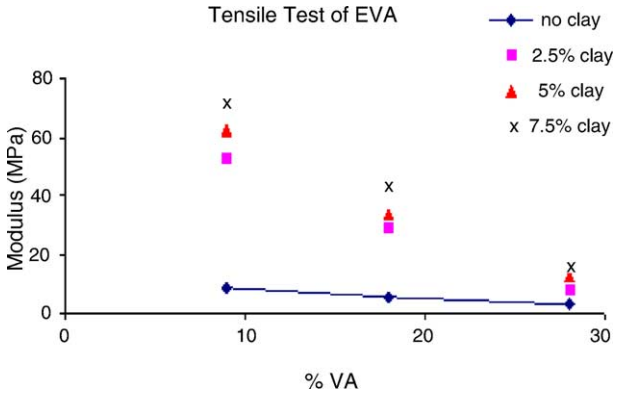

Fig. 14. Tensile modulus variation at different clay concentrations and with increasing matrix amorphicity for EVA PCN family.

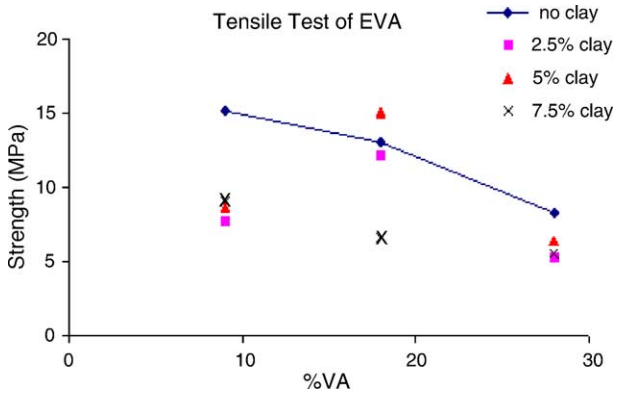

Fig. 15. Tensile strength at different clay concentrations and with increasing matrix amorphicity for EVA PCN family.

lation and (b) an increase in the 'mobile' amorphous phase due to increasing VA content.

Fig. 14 shows that with increasing concentration of nanofiller, there is an increase in Young's modulus (stiffness) of the nanocomposites, as expected. This is because of the typical nanofunctionality of the platelets that impart excellent reinforcement due to an interaction of extremely high surface area of nanoclay with the intercalated polymer that gives excellent filler dispersion [16] and always increases the composite's initial resistance to an applied stress [17].

Though the nanoclay reduces the total crystalline phase of the matrix, large intercalated and exfoliated morphologies increase the above mentioned 'rigid' amorphous phase, and therefore increase the resistance to the movement of polymeric chains under stress [8]. This is most evident with EVA9 and 18 PCNs, since their matrices have comparatively higher resistance (EVA9 having the largest crystalline fraction) and the response diminishes near exponentially with reduction in matrix crystallinity, as shown in Fig. 14, reinforcing the idea that stiffness is largely a crystalline affair and VA pendants cause a 'damping effect' on the stiffness. EVA28, which is completely rubbery, also shows a significant increase (approximately five-fold) in stiffness by mere 7.5 wt.% clay, which is an indication of the level of polymer intercalation and filler–polymer interaction and the formation of 'rigid' amorphous phase. These analyses indicate the significance of understanding the interplay between the matrix amorphicity and clay concentration in determining the nanocomposite mechanical properties.

Fig. 15 shows the tensile strength data for EVA PCNs. The extent to which nanoclay incorporation modifies the PCN morphology can be studied by considering the influence of clay (wt.%) and the effect of increasing VA content simultaneously. Fig. 15 indicates that, in general, addition of nanoclay can suppress the matrix's ability to absorb energy; however, the extent of suppression is significantly influenced by the VA content. The reduction in EVA PCNs strength could be explained by considering that nanoclay increases the spatial hindrance for polymeric chain movement and this is most evident for EVA9, possibly because of the rigidity imparted by the randomly oriented cluster of tactoids that were dispersed in the matrix (TEM from Fig. 4). This macroscopic effect was also explained in the earlier Section 2.3.3 on the basis of a poorly formed microscopic 'network' structure that can interact with the matrix as a whole.

However, if the clay wt.% is increased in the matrix, EVA PCNs show the interesting results. Fig. 15 shows that EVA9 PCNs have an increasing trend with increasing clay concentration, whereas, EVA18 and EVA28 PCNs show an increasing–decreasing trend. The possibility of a flexible clay network structure in the EVA PCNs was mentioned earlier, and this allows the polymeric chain to absorb higher deformational energy by increased alignment and partial transfer due to an intercalation before the chain rupture. This morphological characteristic could explain the increasing–decreasing trend on the basis of type and distribution of clay–polymer clusters, which control the overall matrix deformation capability under stress. WAXS measurements (large basal spacing and presence of shoulder) and TEM support similar morphological characteristic and is in accordance with expectations that with increased polarity, higher polymer–clay interaction are obtained. Thus, EVA18 and EVA28 have greater flexible clay network structure and this results in overall lower percentage reduction in tensile strength as compared to the percent reduction in tensile strength of EVA9. Evidently, better nanocomposites were prepared for EVA18.

4. Conclusions

Clearly, the strong polar interactions between the polymer and the silicate layers of organoclays are critical to the formation of polymer-layered silicate nanocomposites. Though high polarity facilitates greater clay platelet dispersion and achieves mixed intercalated/exfoliated systems, the extent of improvement in the case of tensile modulus and strength is somehow suppressed in spite of the higher specific surface area available for clay–polymer interaction. MDSC results indicate the presence of strong heterogeneous nucleation and

the resulting morphology could be an exfoliation (which was supported by TEM and WAXS studies). However, the morphology was different due to the variation in polar content of the matrix; EVA9 did not show the kind of 'network structure' effect that was shown by EVA18. Avrami fit mostly showed the limited tolerance and indicated a complex nucleation and growth mechanism in most EVA-clay samples (variation in average n was large—from 4 for EVA9 to 2.7 for EVA28). The influence of increasing clay concentration on the tensile behavior of EVA matrices was found to be significant only with low or moderately polar EVA matrix (9% and 18% VA). There is a linear proportionality between clay concentration and tensile modulus for EVA9 and EVA18, a relation not observed with EVA28. Variations in the tensile strength tests are attributed to their sensitivity to the overall interaction of the clay 'network' and the matrix, and for EVA18, there was an increase in tensile strength with 5% clay. WAXS and TEM confirm that degree of dispersion is significantly related to the matrix polarity and their data support the tensile test analysis indicating the presence of strong interactions between the silicate loading and the matrix amorphicity. This study indicated that there is another route for improving the tensile properties of the nanocomposites: by increasing the clay–polymer interaction to an extent that there is a large volume of entangled clay–polymer entities that could significantly increase the resistance of the composite matrix under stress and, at the same time, align themselves in such a fashion that the external stress is distributed over larger fraction of the polymeric chains.

References

[1] G.C. Stael, M.I.B. Tavares, Polym. Test. 16 (1997) 193–198.
[2] D.S. Chaudhary, R. Prasad, R.K. Gupta, S.N. Bhattacharya, Polym. Eng. Sci., 2004, submitted for publication.
[3] T.J. Pinnavaia, G.W. Beall, Polymer–Clay Nanocomposites, John Wiley and Sons, New York, 2000.
[4] C.M.G. De Souza, M.I.B. Tavares, J. Appl. Polym. Sci. 86 (2002) 116–124.
[5] D.S. Chaudhary, M.C. Jollands, F. Cser, Polym. Polym. Compos. 12 (2004) 383–397.
[6] F. Cser, S.N. Bhattacharya, J. Appl. Polym. Sci. 90 (2003) 3026–3031.
[7] A.B. Morgan, J.W. Gilman, J. Appl. Polym. Sci. 87 (2003) 1329–1338.
[8] X. Li, C.S. Ha, J. Appl. Polym. Sci. 87 (2003) 1901–1909.
[9] X. Fu, S. Qutubuddin, Polymer 42 (2001) 807–813.
[10] R. Prasad, R.K. Gupta, F. Cser, S.N. Bhattacharya, Proceedings of the Polymer Processing Society 20th Annual Meeting, Ohio, USA, 2004, Paper 256.
[11] J.W. Gilman, T.Kashiwagi, A.B. Morgan, R.H. Harris, L.Brassell, M.Van Landingham, C.L. Jackson, NIST Internal Report 6531, National Institute of Science and Technology, 2000.
[12] L. Liu, Z. Qi, X. Zhu, J. Appl. Polym. Sci. 71 (1998) 1133–1138.
[13] R.A. Vaia, B.B. Sauer, O.K. Tse, E.P. Giannelis, J. Polym. Sci. B: Polym. Phys. 35 (1997) 59–67.
[14] S.W. Lee, M. Ree, C.E. Park, Y.K. Jung, C.S. Park, Y.S. Jin, D.C. Bae, Polymer 40 (1999) 4737–7146.
[15] Y. Li, G. Zhang, X. Zhu, D. Yan, J. Appl. Polym. Sci. 88 (2002) 1311–1319.
[16] M. Alexandre, P. Dubois, Mater. Sci. Eng. Rep. 28 (2000) 1.
[17] J.M. Hauldin, in: C. Bescaig (Ed.), Plastic Deformation of Amorphous and Semi-Crystalline Materials, Les Editions de Physique, Paris, 1982.